

# FPGA-based Smart Sensor for Detection and Classification of Power Quality Disturbances using Higher Order Statistics

Gerardo de J. Martinez-Figueroa, Daniel Morinigo-Sotelo, *Member, IEEE*, Angel L. Zorita-Lamadrid, Luis Morales-Velazquez, *Member, IEEE*, and Rene de J. Romero-Troncoso, *Senior Member, IEEE*

**Abstract**—Power quality (PQ) has received the attention of several research groups due to the impact of PQ disturbances (PQD) and how they affect the operation of the electrical equipment connected to the grid, especially in industrial and healthcare facilities. The monitoring and analysis of PQD are generally performed with specialized measuring equipment such as power analyzers based on the standards. However, this equipment is not suited to perform continuous monitoring and classification of PQD, and it cannot be configured to perform further analysis of the monitored signal. Smart sensors, on the other hand, can provide the functionality that the standard equipment cannot, by integrating several signal processing modules that can be reconfigured using a reconfigurable technology such as field programmable gate arrays (FPGA). This paper presents the development of an FPGA-based smart sensor that integrates the processing cores of higher-order statistics (HOS) to provide a signal analysis aimed to detect and quantify PQD on electrical installations, and an artificial neural network (ANN) to classify the PQD. Experimentation is performed on the electrical installation in hospital facilities. Results from the HOS processing of electrical signals show that these processing methodologies are suitable for the quantification and classification of PQD on electrical installations.

**Index Terms**—Field programmable gate arrays, higher order statistics, artificial neural networks, power quality, sensor systems and applications.

## I. INTRODUCTION

**E**LECTRIC power is considered a primary resource due to the number of industrial activities that depend on it. In addition to providing energy for lighting and air conditioning, it drives electric motors with a wide variety of applications: lifts, milling machines, grinders, mixers, pumps, compressors, lathes as well as other machine tools. The primary function of

a power supply system is to feed loads economically and with appropriate levels of continuity and quality. Continuity means an uninterrupted power supply service. The term power quality (PQ) refers to a variety of electromagnetic phenomena that characterize the voltage and the current, in a particular time and place, within the power supply system [1]. The classification and identification of power quality disturbances (PQD) are defined in standards such as the IEEE 1159 [2], the IEC 61000-4-30 [3] and the EN 50160 [4]. The use of standards is necessary to homologate the definitions and classifications of PQD and to have a recommended practice for monitoring. There are two main approaches for PQ monitoring [5]: the development of indices to quantify the PQ, and the PQD detection and classification in harmonics, sags, swells, interruptions, transients, voltage fluctuations, notching, power frequency variations and so forth. Tools for the detection and classification of PQD are essential in industrial applications.

PQ has become an important requirement for industrial facilities, public buildings, and homes mainly due to economic reasons. Firstly, in all electricity supply companies, meeting the customer expectations and maintaining customer confidence are strong motivations to keep a high-quality electrical supply. With the recent movement towards deregulation and competition between service providers, the loss of disgruntled customers due to a competing provider with better PQ can have a significant financial impact. Besides, the presence of PQD on the power supply causes a low power factor, which is penalized for industries, along with the increased power demand. Another undesired effect of PQD is the high sensitivity of electronic devices to the disturbances [6], which produces a degradation of the equipment performance. This is true, no matter if the equipment is a computer in an office, an ultrasonic imaging machine in a hospital, or a process controller in a manufacturing plant [7]. For instance, the manufacturing industry makes use of rotatory machines like lathes and milling centers. These machines are mechanically driven by electric motors that are mostly induction motors (IM). It has been demonstrated that the PQ of the electric supply feeding the electric motors of manufacturing machines can affect the production process and the quality of the manufactured workpiece [8]. Effects on equipment and process operations can include missing operation, damage, process disruption, efficiency and life expectancy decreasing, among other anomalies. The standard

This work was supported in part by CONACYT Scholarship 401359; by Universidad de Guanajuato, DAIP, under Grant 733/2016, and by a grant from CEI Triangular-E3: Universidades de Burgos, León y Valladolid.

G. de J. Martinez-Figueroa is with Universidad de Guanajuato, Salamanca, Gto., 36885 Mexico (e-mail: gdj.martinezfigueroa@ugto.mx).

D. Morinigo-Sotelo and A.L. Zorita-Lamadrid are with Universidad de Valladolid, Valladolid, Spain (e-mail: dmorinigo@hspdigital.org and zorita@eii.uva.es).

L. Morales-Velazquez is with Autonomous University of Queretaro, San Juan del Rio 76806, Mexico (e-mail: lmorales@hspdigital.org).

R. de J. Romero-Troncoso is with Universidad de Guanajuato, Salamanca, Gto., 36885, Mexico (Corresponding autor e-mail: troncoso@hspdigital.org).

IEEE-1159 has a section about the specific effects on equipment, classified by the type of PQD that affects the PQ. Among the phenomena that cause PQD are non-linear loads, switching power supplies, transformers, high-power commutation, power inverters, and electric motors operating in a faulty condition. For all the reasons above, it is relevant the continuous monitoring of the PQ and the detection and classification of the PQD that are present in the power line. Monitoring also may be used to diagnose the equipment condition and predict future performance of the attached loads.

Instruments used for PQ monitoring can range from a simple voltmeter to a sophisticated PQ monitoring system which is not common to be permanently installed. The selection of the measurement device for monitoring depends on the signal processing algorithms to be performed and its location. Among the most common commercial monitoring tools are digital handled and bench multi-testers, power analyzers and spectrum analyzers. In [9], authors make a comparative analysis of commercial PQ instruments for measuring voltage and power consumption. They apply distorted three-phase voltage signals to several kinds of PQ monitoring instruments, considering harmonics, sags, swells, and unbalanced voltages. Next, the features of these PQDs are measured, compared and evaluated taking into account the different instruments under analysis. They conclude that the instruments present different results for the same kind of PQD due to the absence of standardization of measurement protocols. Authors suggest that more research is necessary to develop new and smarter devices for PQ monitoring with better performance, precision, and accuracy. A review of PQ monitoring systems is presented in [10]. The authors state that some of the investigations were carried out to develop efficient PQ monitoring systems to find the best location for meters in the electrical grid, which will help to improve the PQ monitoring system. Each PQ monitoring system is analyzed regarding its advantages, disadvantages, monitoring schemes, and the PQD detected and classified. No actual PQ monitoring systems of this survey can detect and classify all the PQD present on the power line, and this results in real limitations. Industrial monitoring systems require high-performance instrumentation, low-cost primary sensors and online signal processing for a real-time monitoring [11].

A very useful technological tool that integrates all these characteristics is the smart sensor [12]. From a technological point of view, a smart sensor is a system that includes, at least, a primary sensor, integrated signal conditioning and processing capabilities, and communication [13]. Besides, according to [14]-[16], a smart sensor can also incorporate data logging, learning, decision making and an embedded power source. One of the most promising options for designing and implementing affordable smart sensors is the field programmable gate array (FPGA), due to their inherent parallelism, high-performance, reconfigurability and low cost [17], [18]. On an FPGA, several methods of signal processing can be implemented at the same time, thanks to its parallelism. This is important towards implementing all the methodologies necessary to detect and classify online as many PQD as possible, where most of actual PQ monitoring systems are limited.

Several smart sensors for power measurement, PQ monitoring, and PQD detection and classification have been recently developed. An FPGA-based measurement instrument for PQ monitoring in compliance with the IEC standards is presented in [19]. The instrument applies a digital filter approach, only for harmonic and interharmonic estimation, but the authors conclude that the obtained results can be extended to the evaluation of other PQ parameters. A high-speed hardware-efficient digital system, based on the wavelet transform for real-time fault detection and classification in transmission lines is reported in [20]. The digital system is implemented in an FPGA, achieving high-speed and real-time processing. In [21], it is proposed a Hilbert transform-based smart sensor for detection, classification, and quantification of single PQD, using only a voltage divider as a primary sensor. The Hilbert transform (HT) is used as a detection technique, and later, an artificial neural network (ANN) performs the classification of the PQD using the envelope provided by the HT. Finally, some PQ indices are calculated through the HT and Parseval's theorem to quantify the PQD. A system of smart sensors and actuators for power management in intelligent buildings is proposed in [22]. In [23], they present an FPGA-based ANN harmonic estimation for continuous monitoring of the power line. This methodology allows the analysis during the transient or the steady state of a signal, giving a better time-frequency resolution than the classical techniques. The implemented ANN gives a time-evolution of harmonics and interharmonics for amplitudes and phases. A real-time hardware platform for PQD classification is presented in [24]. It is based on the S-transform and dynamics and can classify ten types of single or combined PQD. The development of FPGA-based smart sensors has been recently significant, including some smart sensors for PQ monitoring and PQD detection and classification. However, there are still possibilities to make contributions in this field. These are based on the integration of signal processing capabilities in the smart sensor that has not been previously considered like higher-order statistics (HOS), which have been proven to be useful for signal parameterization and characterization towards the detection and classification of PQD.

Most of the developed smart sensors for PQ monitoring and PQD detection are based on techniques that work on the frequency-domain. There are very few smart sensors that work in the time-domain for these purposes, and there is a lack of the development of smart sensors that can parameterize and characterize a signal using HOS for applications on the PQ monitoring. Recently, the HOS have wide applicability in many diverse fields; e.g., sonar, radar, plasma physics, biomedicine, seismic data processing, image reconstruction, time-delay estimation, adaptive filtering, array processing, blind equalization, harmonic retrieval, spectral analysis and telecommunications [25]. The HOS also have applications in monitoring and diagnosing PQD. De la Rosa use the spectral kurtosis in [26] to characterize PQD. In [27], the authors present a virtual instrument that uses the variance, skewness, kurtosis and case-based reasoning to detect sags, swells, 50 Hz asymmetries, and non-50 Hz events. In [28], the authors use the power spectral density ratio, variance, maximum gradient, percentage distortion, skewness, kurtosis, Pearson correlation and Shannon entropy to extract features of voltage signals and

classify PQD using support vector machines (SVM). Their methodology can detect and classify sags, swells, transients, harmonics, outages and its hybrids. In [29], it is reported an FPGA-based system for the spectral kurtosis calculation, with a prospective application to harmonic detection. All these developments with HOS do not cover all types of PQD and do not work online or in real time.

The main contribution of this work is the development of an HOS-based smart sensor for online PQ monitoring and detection and classification of PQD in noisy environments of electrical installations with severe interference and distortions, as it happens in the healthcare facilities. Another significant contribution is the simplicity of the proposed methodology and the low computational complexity of the smart sensor. The smart sensor is implemented on an FPGA for a continuous and online operation at low cost. It is designed to specifically compute the mean, variance, skewness and kurtosis of voltage and current signals for PQ monitoring. Later, the features of the voltage signals are used in an ANN for the PQD classification stage. The smart sensor is applied to electric signals of a three-phase electrical system at a healthcare facilities. Previously, the smart sensor is calibrated with known and controlled signals in a laboratory. The results show that the HOS-based smart sensor provides useful information for PQ monitoring and detection and classification of PQD.

## II. THEORETICAL BACKGROUND

### A. Power Quality Disturbances

PQD are distortions in voltage or current that present unexpected variations in magnitude concerning nominal values during a time interval. The classification and identification of each disturbance are usually carried out using standards and recommendations like the IEEE 1159 and EN 50160. These standards classify the PQD depending on their spectral content, duration, and magnitude into seven categories: transients, short duration root-mean-square (RMS) variations, long duration RMS variations, imbalance, waveform distortion, voltage fluctuations and power frequency variations. The first category includes two transient types: impulsive and oscillatory. Sags, swells, and interruptions are included in the category of short-duration RMS variations. The category of long-duration variations is added to deal with ANSI C84.1 limits [30] and includes under-voltages, over-voltages, and current overloads. The fourth class includes voltage and current imbalances. The waveform distortions category includes harmonics, inter-harmonics, noise, notching and direct current (DC) phenomena in alternate current (AC) networks. The last two categories only include voltage fluctuations and power frequency variations, respectively. Table I shows the characteristics of the most common PQD. Fig. 1 depicts the waveforms of these PQDs.

### B. Higher-order Statistics

Recently, HOS are widely used to deduce newly statistical features from the data of time-series measurements. These statistics are especially useful in problems where either non-

TABLE I  
CHARACTERISTICS OF COMMON PQD

PQD	Typical spectral content (kHz)	Typical duration	Magnitude (pu)
Sag	-	0.5 cycles - 60 segs	0.1-0.9
Swell	-	0.5 cycles - 60 segs	1.1-1.8
Interruption	-	0.5 cycles - 60 segs	<0.1
Impulsive transient	-	0.000005 ms - 0.1 ms	-
Oscillatory transient	<5000	0.005-50 ms	0-8
Voltage fluctuations	<25	Intermittent	0.001-0.07
Notching	-	Steady state	-
Harmonics	0-9	Steady state	0-0.2

The quantity *pu* refers to *per unit*, which is dimensionless. The nominal rms value is used as the base for PQD, except for oscillatory transient, for which the nominal peak value is used.

Gaussian, non-minimum phase, colored noise, or nonlinearities are important and must be considered.

In mathematics, the arithmetic mean is defined as the sum of a collection of numbers divided by the total of numbers in the collection. In this context, the mean or expected value of a time-series or a random variable is a measure of its central tendency, either of a probability distribution or the random variable that characterizes the time-series. Therefore, the expected value  $E[x]$  of the discrete time-series or random variable  $x(k)$  of  $N$  samples, is given by (1).

$$E[x] = \frac{1}{N} \sum_{k=1}^N x(k) \quad (1)$$

The  $n^{\text{th}}$ -order cumulant is defined in terms of its joint moments of orders up to  $n$ . For zero-mean real random variables, the second, third and fourth order joint cumulants are respectively given in [25] as (2) to (4), where  $E[x]$  is the expected value operator.

$$\text{Cum}(x_1, x_2) = E[x_1 x_2] \quad (2)$$

$$\text{Cum}(x_1, x_2, x_3) = E[x_1 x_2 x_3] \quad (3)$$

$$\begin{aligned} \text{Cum}(x_1, x_2, x_3, x_4) = & E[x_1 x_2 x_3 x_4] - E[x_1 x_2]E[x_3 x_4] \\ & - E[x_1 x_3]E[x_2 x_4] - E[x_1 x_4]E[x_2 x_3] \end{aligned} \quad (4)$$

In the case of nonzero mean real random variables,  $x_i$  is replaced by  $x_i - E[x]$  in (2), (3) and (4). Consider  $\{x(k)\}$ , as a zero-mean  $n^{\text{th}}$ -order stationary and real stochastic process; the  $n^{\text{th}}$ -order cumulants defined as the joint  $n^{\text{th}}$ -order cumulant of the random variables  $x(k), x(k + \tau_1), \dots, x(k + \tau_{n-1})$ , i.e. [25]:

$$C_{n,x}(\tau_1, \dots, \tau_{n-1}) = \text{Cum}(x(k), x(k + \tau_1), \dots, x(k + \tau_{n-1})) \quad (5)$$

where  $\tau_i$  are time-shifts, and the  $i^{\text{th}}$ -shifting is a multiple of the data acquisition sampling period  $T_s$ .

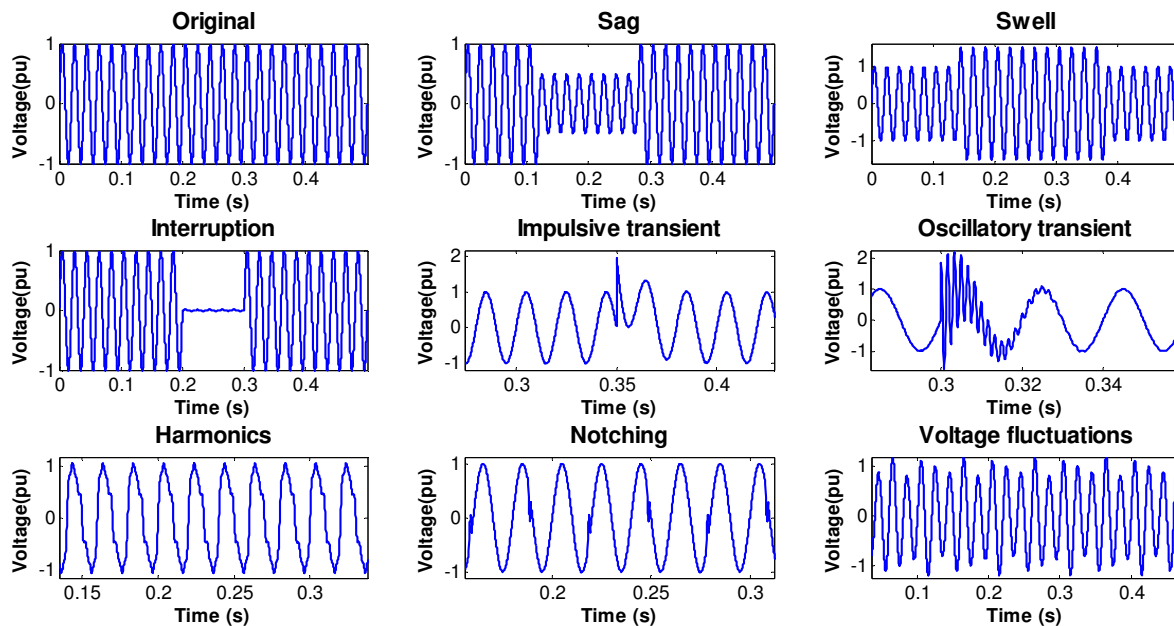


Fig. 1. Waveforms of several common PQD.

The particular cases for the second-, third- and fourth-order cumulants for a zero-mean and stationary discrete time-series  $x(k)$ , can be estimated respectively by [25]:

$$C_{2,x}(\tau) = E[x(k)x(k + \tau)] \quad (6)$$

$$C_{3,x}(\tau_1, \tau_2) = E[x(k)x(k + \tau_1)x(k + \tau_2)] \quad (7)$$

$$C_{4,x}(\tau_1, \tau_2, \tau_3) = E[x(k)x(k + \tau_1)x(k + \tau_2)x(k + \tau_3)] - C_{2,x}(\tau_1)C_{2,x}(\tau_2 - \tau_3) - C_{2,x}(\tau_2)C_{2,x}(\tau_3 - \tau_1) - C_{2,x}(\tau_3)C_{2,x}(\tau_2 - \tau_1) \quad (8)$$

where again  $\tau_1$ ,  $\tau_2$ , and  $\tau_3$  are the time-shifts. As in (2), (3) and (4),  $x(k)$  is replaced by  $x(k) - E[x(k)]$  in (6), (7) and (8) for nonzero mean time-series. Each cumulant can be interpreted as a correlation among the original time-series and its associated time-shifted versions. By suppressing time shifting,  $\tau = \tau_1 = \tau_2 = \tau_3 = 0$ , in (6), (7) and (8), leads to

$$\gamma_{2,x} = C_{2,x}(0) = E[x^2(k)] \quad (9)$$

$$\gamma_{3,x} = C_{3,x}(0) = E[x^3(k)] \quad (10)$$

$$\gamma_{4,x} = C_{4,x}(0) = E[x^4(k)] - 3(\gamma_{2,x})^2 \quad (11)$$

The ensemble of (9), (10) and (11) constitutes indirect measures of the variance, skewness, and kurtosis [27]; these statistics are more known than cumulants. Of course, if the time-series  $x(k)$  is non-zero mean, the mean has been subtracted from it. For skewness and kurtosis, normalized quantities are defined as  $\gamma_{3,x}/(\gamma_{2,x})^{3/2}$  and  $\gamma_{4,x}/(\gamma_{2,x})^2$ , respectively. The variance, skewness and kurtosis are redefined in (12), (13) and (14). Normalization makes estimators shift and scale invariant. If  $x(k)$  is symmetrically

distributed, its skewness is zero (but not *vice versa*); if  $x(k)$  is Gaussian distributed, its kurtosis is zero (but not *vice versa*).

$$\gamma_{2,x} = E[x^2(k)] - \mu^2 \quad (12)$$

$$\gamma_{3,x} = \frac{E[(x(k) - \mu)^3]}{E[(x(k) - \mu)^2]^{3/2}} \quad (13)$$

$$\gamma_{4,x} = \frac{E[(x(k) - \mu)^4]}{E[(x(k) - \mu)^2]^2} - 3 \quad (14)$$

### C. Artificial Neural Networks

According to [31], an ANN is a machine designed to model the way in which the brain performs a particular task or function of interest. In this case, the task of interest is the classification, performed by a process of learning. An ANN consists of simple processing units, called neurons, and directed connections between them, characterized by a weight. There are some types of ANN according to its architecture. A feed-forward neural network (FFNN) is a type of ANN characterized by having layers clearly separated, with single or multiple neurons in each layer [32], as shown in Fig. 2(a). In this architecture, the input information moves in one direction only, and the connections are only permitted to neurons of the following layer. The typical model of a neuron is described by (15) and the diagram of Fig. 2(b).

$$y = f\left(\sum_{i=1}^l \omega_i x_i + b\right) \quad (15)$$

The model of the neuron consists of the summation  $\Sigma(\cdot)$  of the multiplications between the inputs  $x_i$  and the associated weights  $\omega_i$ , plus a bias  $b$ ; then, this result is evaluated with a nonlinear function  $f(\cdot)$  to provide the FFNN with the ability to model nonlinear relationships [33].

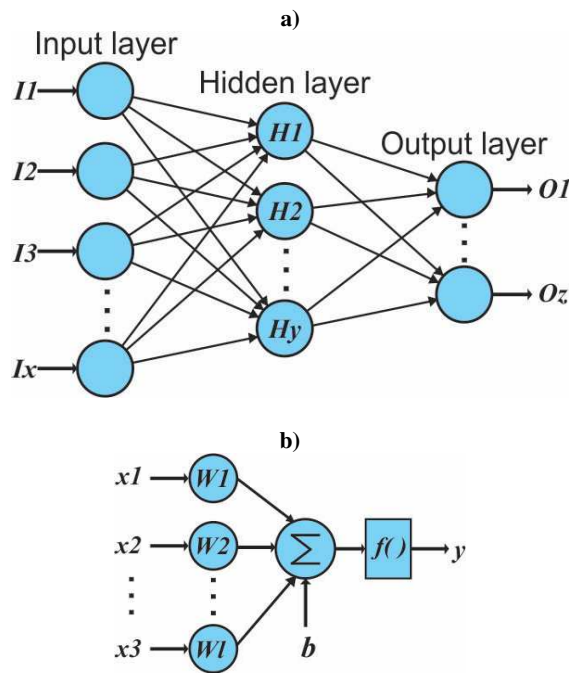


Fig. 2. Feed forward neural network. a) Architecture; b) Nonlinear model of neuron.

### III. METHODOLOGY

This section shows the smart sensor and the proposed methodology implemented in the FPGA-based processor for achieving the PQ monitoring and the detection and classification of PQD.

#### A. Smart sensor

The block diagram of the smart sensor architecture is shown in Fig. 3. The smart sensor is divided into three stages: primary sensors, a data acquisition system (DAS) and an FPGA-based processor. It is designed for three voltage signals and three current signals of a three-phase system.

In the primary sensor stage, there are six sensors divided into two types: three voltage sensors and three current sensors. The voltage sensors are voltage dividers, whereas the current sensors are AC FLUKE i400s current clamps with a measurement range from 0 to 400 A. The primary sensors are connected to a proprietary DAS consisting of a signal conditioning stage and an analog-to-digital converter (ADC). The signal conditioning stage consists of a fully-differential isolation amplifier, model AMC1200, to get electrical isolation between the power system and the smart sensor, and a low-pass anti-aliasing filter of second order with a cutoff frequency of 3043.7 Hz, allowing the correct analysis of harmonics and PQD with frequencies lower than it. Afterward,

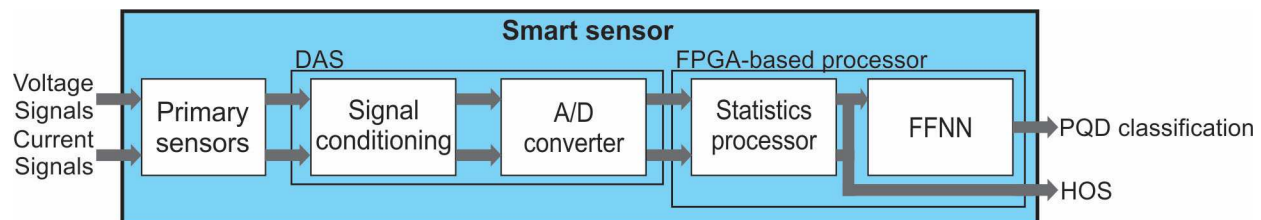


Fig. 3. Architecture of the proposed smart sensor.

the conditioned signals are digitally acquired with 16-bit resolution using an ADS130E08 from Texas Instruments, which can acquire data simultaneously from eight channels at 8000 samples per second (SPS). The DAS also has an integrated data logger, which is developed for acquiring and collecting data from the measured physical variables. The DAS has the advantage of being non-intrusive, and it is easily attached to the desired power line to acquire instantaneous current and voltage signals preserving their original waveforms at the point of interest with a storage capacity of over seven days of continuous acquisition. It is used to provide the FPGA-based processor the voltage and current signals of one phase of a power system. The developed DAS is first calibrated using a reference equipment. Then, the methodology is validated in a controlled installation facility by acquiring data with the developed DAS and the reference equipment.

The FPGA-based processor is the final stage of the smart sensor, which is responsible for the PQ monitoring and detection and classification of PQD, performed by the HOS processing cores and an FFNN. This processor delivers the classified PQD and the HOS to the user through a liquid crystal display (LCD) or an optional personal computer (PC).

#### B. DAS calibration

The calibration process of the proprietary DAS is shown in the chart flow of the Fig. 4. First, the DAS is placed in parallel with a reference instrument to acquire three-phase voltages and currents of a test bench consisting of three balanced, star-connected loads. The first load bank is purely resistive, the second load bank is purely capacitive, and the third load bank is mostly inductive by connecting an unloaded 2.2 kW three-phase induction motor.

The real power consumption estimation  $P_S$  is calculated for each phase for a time lapse of one minute. In (16),  $\tau$  is the moment when the measurement starts,  $k$  is a positive integer number,  $T_0$  is the cycle time, and  $p$  is the instantaneous power, calculated as the  $v \cdot i \cdot \cos(\theta)$  product, where  $v$  is the instantaneous voltage,  $i$  is the instantaneous current and  $\theta$  is the phase.

$$P_S = \frac{1}{kT_0} \int_{\tau}^{\tau+kT_0} p dt \quad (16)$$

The real power consumption estimated by the DAS is compared to the reference instrument and from the statistical analysis of the acquired data in both systems; the calibration error  $E_{rr}$  of the DAS are estimated according to (17),

$$E_{rr} = \sqrt{\frac{\sum d^2}{n}} * 100\% \quad (17)$$

where  $d$  is the difference between the power value estimated by the reference and the value obtained with the DAS, and  $n$  is the number of samples of the acquired signal. For the calibration process, the DAS estimates the power consumption by applying the standard IEEE 1459 stated in (16).

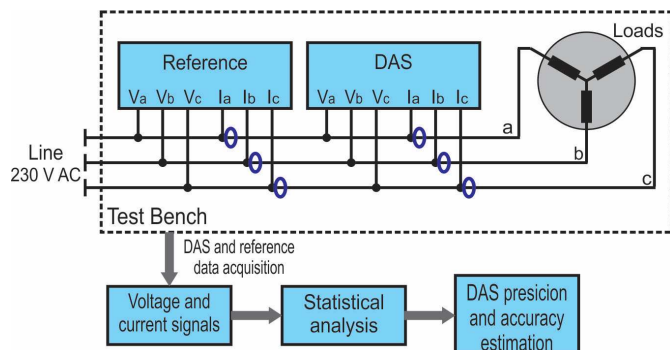


Fig. 4. Flow chart of DAS calibration process.

### C. FPGA-based processor

Fig. 5 depicts the block diagram of the general FPGA-based processor architecture. This diagram shows only the architecture for a single signal of a single-phase, but it is replicated in parallel for the two signals (voltage and current) of the three phases. The FPGA-based processor consists of two main stages. The first stage contains the HOS processing cores, which are responsible for the PQD detection and PQ monitoring. There are four cores for the HOS computing: mean, variance, skewness, and kurtosis.

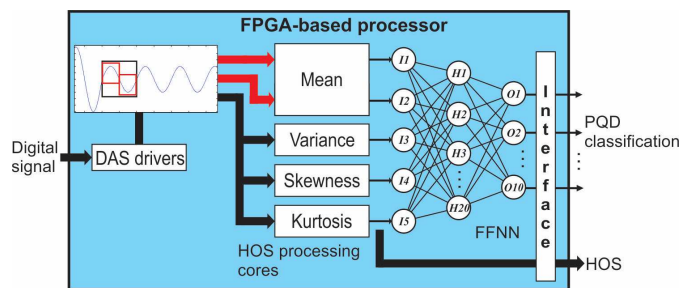


Fig. 5. General architecture of the FPGA-based processor.

The processing cores obtain the HOS of each signal cycle at each work cycle, except for the mean that is obtained twice at each work cycle, one for each half signal cycle, which makes a total of five voltage signal features and PQ indices. These processing cores are fully implemented on a single FPGA. To keep the overall cost of the system low and to comply with the processing speed requirements, all the processing cores were fully developed by the authors under Very high speed integrated circuit Hardware Description Language (VHDL), and commercially available processing cores were not used.

The most basic HOS processing core is the mean core, whose architecture is depicted in the block diagram of Fig. 6. It is based on a digital structure known as the accumulator. This structure consists of an adder and two registers. Both register inputs are connected to the adder output, whereas one

register output is connected in feedback to the adder input. The function of this structure is to compute successive sums using only one adder. After the accumulator, a divider structure is used to divide the sum of all samples of the input signal  $x(k)$  between the number of samples  $N$ , obtaining the  $Y$  output, which is the mean according to (1). The divider is a digital structure based on a successive approximations register (SAR). This divider computes the division using a successive approximations approach. The SAR successively approximates the quotient value, comparing the quotient and divisor product ( $B*Y$ ), with the  $A$  dividend, until the product value is equal or very close to the dividend value.

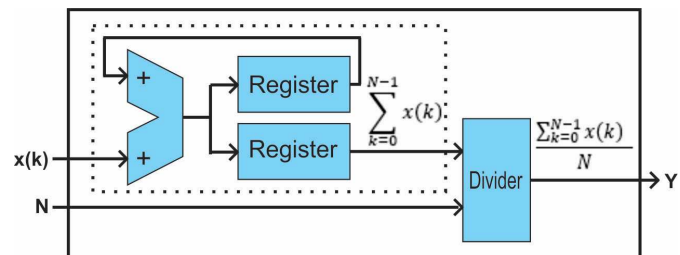


Fig. 6. Architecture of the processing core for computing the mean.

Fig. 7 shows the block diagram that depicts the architecture of the processing core for computing the variance according to (12). This core is based on a digital structure known as the multiply-accumulator (MAC) and consists of a multiplier, an adder, and two registers. Its function is to compute the product of two numbers and adds that product to an accumulator, therefore computing the successive sum of products. This structure is used to compute, together with the divider, the first part of (12),  $E[x^2(k)]$ . Also, an accumulator is used to help in the computing of the mean, while a multiplier obtains its second power, which is the second part of (12),  $\mu^2$ .

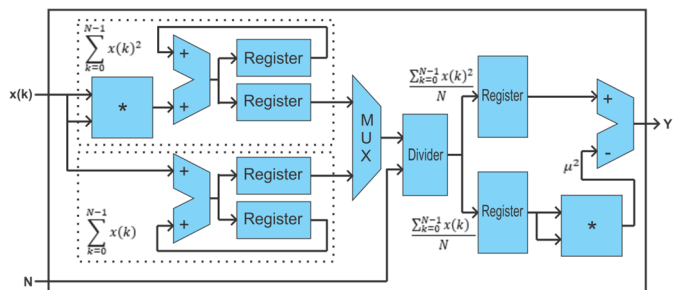


Fig. 7. Architecture of the processing core for computing the variance.

The third processing core computes the skewness, and its architecture is depicted in the block diagram of Fig. 8, according to (13). A new digital structure is used in this core, named serial multiplier. This structure computes a product with more than two multiplicands, using only one multiplier and a register. It is used to obtain the third power,  $(x(k)-\mu)^3$ , and the second power,  $(x(k)-\mu)^2$ . After, two accumulators compute the sum of all previous products or powers, and two dividers are used to obtain the means  $E[(x(k)-\mu)^3]$  and  $E[(x(k)-\mu)^2]$ . Another new structure in the skewness core is the square root structure, which makes use of the same successive approximations approach than the divider. This unit, along

with a serial multiplier, obtains  $E[(x(k)-\mu)^2]^{3/2}$ . At the end, a divider computes the division  $E[(x(k)-\mu)^3]/E[(x(k)-\mu)^2]^{3/2}$ . The skewness core also uses a random access memory (RAM), because it needs to store the signal samples to subtract later the mean to each one.

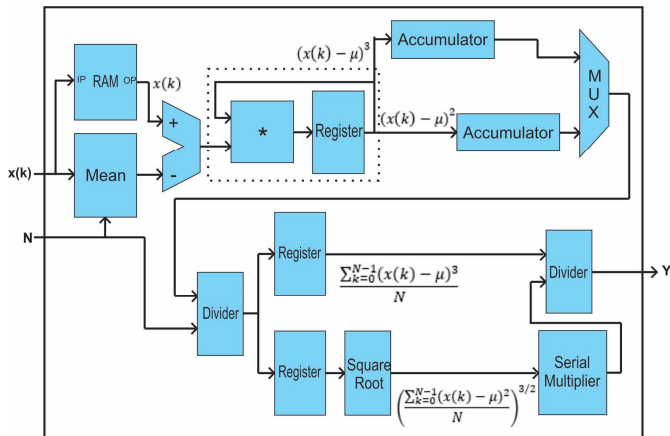


Fig. 8. Architecture of the processing core for computing the skewness.

The last processing core is for computing the kurtosis. The block diagram in Fig. 9 shows its architecture, according to (14). There are no new digital structures, compared to previous cores. A serial multiplier obtains the powers  $(x(k)-\mu)^4$  and  $(x(k)-\mu)^2$ . Later, two accumulators and two dividers compute the expected values  $E[(x(k)-\mu)^4]$  and  $E[(x(k)-\mu)^2]$ , and a multiplier obtains the square of the last one. At the end of the core, a divider computes the division  $E[(x(k)-\mu)^4]/E[(x(k)-\mu)^2]^2$ , and a constant value of three is subtracted from it to obtain the kurtosis.

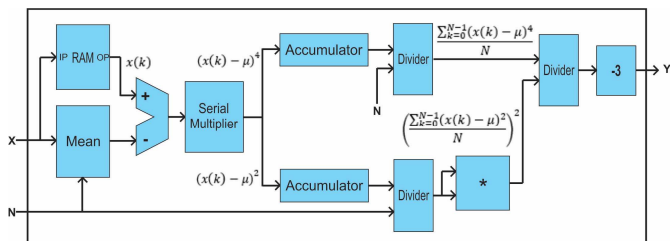


Fig. 9. Architecture of the processing core for computing the kurtosis.

After the detection and monitoring stage, the classification stage is carried out by an FFNN using the five voltage signal features previously computed. Hence, the FFNN has five inputs, twenty neurons in the hidden layer and ten outputs. After each work cycle, during which a signal cycle is analyzed, the FFNN indicates the type of PQD through its ten outputs. The ten outputs are one per each PQD (sag, swell, interruption, impulsive transient, oscillatory transient, voltage fluctuations, notching, harmonics, harmonics plus sag and harmonics plus swell) since each neuron is set at one if the PQD exists and to zero when there is no PQD. As it is known, the output of an FFNN is rarely exactly zero or one. Therefore, a threshold of 0.5 is used to force the outputs either to zero or to one, respectively. The digital structures of the FFNN and its architecture in the FPGA-based processor are shown in [34].

## IV. EXPERIMENTATION AND RESULTS

This section presents the DAS calibration setup, and its results. The validation and the experimental setup for evaluating the performance of the proposed smart sensor are also presented.

### A. DAS calibration setup

During the calibration of the smart sensor, the reference instrument used is a three-phase power analyzer FLUKE 434 [35] with FLUKE i400s AC current clamps. Three different loads are used for calibration; the first is a three-phase bank of purely resistive loads of 71  $\Omega$ ; the second load is a three-phase bank of purely capacitive loads of 75  $\mu\text{F}$ , and the third one is an unloaded three-phase induction motor representing a mostly-inductive load of 560 mH. The loads are connected to a 230 V<sub>AC</sub> and 50 Hz supply. The test time for every load is set to 10 minutes, where the DAS and the reference instruments are working simultaneously. The acquired data are processed to obtain the mean and standard deviation of the DAS comparing to the reference instrument to estimate the error of the DAS in order to calibrate it. Fig. 10 shows the calibration setup.

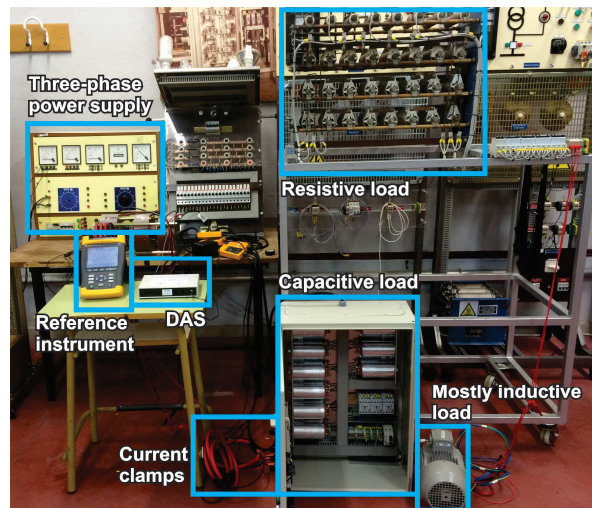


Fig. 10. DAS calibration setup in laboratory.

The measurement error resulting from the calibration process in the three-phase load test bench is 1.9% for phase 1, 0.61% for phase 2, and 0.98% for phase 3. According to the estimated error, a mean ratio between the power consumption estimation of the reference and the DAS is obtained. This mean ratio of 0.9825 is the DAS gain adjustment factor. Applying this correction factor to the DAS, the measurement error is reduced to 0.04% for phase 1, 0.04% for phase 2, and 0.03% for phase 3.

### B. Training and validation

Firstly, a database of 2200 synthetic signals is generated, 200 for each one of the ten PQD aforementioned, plus 200 pure signals. These signals, of one cycle of duration, are generated according to the mathematical models shown in Table II, with random parameters within the established limits [36], [37]. The 200 signals for each PQD are separated into 100 for training and 100 for validating the proposed

TABLE II  
PQD MATHEMATICAL MODELS

PQD	Equation (Pure signal + PQ Disturbance)	Parameters
Pure signal	$x_1(k) = A * \sin(2\pi f k)$	$f = 50 \text{ Hz};$ $0.9 \leq A \leq 1.1$
Sag	$x_2(k) = A[1 - \alpha(u(k - k_1) - u(k - k_2))] \sin(2\pi f k)$	$0.1 \leq \alpha \leq 0.9; k_1 < k_2$
Swell	$x_3(k) = A[1 + \alpha(u(k - k_1) - u(k - k_2))] \sin(2\pi f k)$	$0.1 \leq \alpha \leq 0.8; k_1 < k_2$
Interruption	$x_4(k) = A[1 - \alpha(u(k - k_1) - u(k - k_2))] \sin(2\pi f k)$	$0.9 \leq \alpha \leq 1.0; k_1 < k_2$
Impulsive transient	$x_5(k) = A * \sin(2\pi f k) + \alpha * \exp(-\beta(k - k_1)) u(k - k_1)$	*
Oscillatory transient	$x_6(k) = A * \sin(2\pi f k) + \alpha * \exp[-\beta(k - k_1) * \cos(2\pi f_2 k)] u(k - k_1)$	$0 < \alpha \leq 4A;$ $100 \leq \beta \leq 350;$ $f_2 \leq 4000 \text{ Hz}$
Voltage fluctuations	$x_8(k) = A[1 + \alpha \sin(2\pi f_2 k)] \sin(2\pi f k)$	$0.001 \leq \alpha \leq 0.07;$ $f_2 \leq 25 \text{ Hz}$
Notching	$x_7(k) = A \sin(2\pi f k) - \alpha \{ \text{sign}(\sin(2\pi f k)) \llbracket \sin(2\pi f_2 k) \rrbracket \}$	$0.1 \leq \alpha \leq 0.4;$ $100 \leq f_2 \leq 500 \text{ Hz}$
Harmonics	$x_9(k) = A * \sin(2\pi f k) + \sum_{i=2}^N A_i * \sin(2\pi i f k)$	$A_i \leq 0.2A$

$u[\ ]$ : Step function.  $\llbracket \ ]$ : Round function. \* Not defined.

methodology. In the equations of Table II,  $A$  is the amplitude of the pure signals without PQD and  $f$  is the fundamental frequency. In the sag, swell, interruption, and transient equations,  $\alpha$  is the disturbance amplitude, while  $A_i$  are the harmonics amplitudes. In the equations of transient PQD,  $\beta$  is known as the time constant, while in the voltage fluctuations equation, is known as the modulation index. In the oscillatory transient equation,  $f_2$  is the transient frequency, whereas, in the voltage fluctuation equations, is the modulation frequency. In all PQD equations,  $k_1$  and  $k_2$  are respectively the initial and final discrete times of the PQD.

Regarding the FFNN structure and training, a log-sigmoid activation function is used. The training goal is set at 0, the training rule is the Levenberg-Marquardt algorithm, and a maximum of 1000 epochs and/or 50 validations failures are allowed. All the aforementioned are carried out offline using the MATLAB software; once the FFNN is built, trained, and validated, their weights and biases are used in the digital structures in the FPGA-based processor. The overall methodology is implemented and validated using the MATLAB software. Table III shows the classification PQD results in noiseless conditions. The first column indicates the kind of PQD, while the respective row indicates the number of samples classified in each category. Table IV shows the HOS obtained for each kind of PQD. This table shows the PQ monitoring through the mean values and standard deviations of each HOS. The first two columns show the mean of the positive half cycle of each synthetic signal, the next two, the mean of the negative half cycle, and the next columns show the variance, skewness and kurtosis, respectively.

### C. Experimental setup

On the other hand, the methodology for PQ monitoring implemented on the smart sensor is tested under real operating conditions, specifically with voltage and currents signals acquired from a 230 V<sub>AC</sub> and 50 Hz three-phase power system of a healthcare facility. The developed smart sensor is shown in Fig. 11, whose processor is implemented into a proprietary FPGA EP4CE115F29C7 of the Cyclone IVE family, in an Altera DE2-115 development board [54] running at 50 MHz.

Table V summarizes the resources usage of the FPGA and the maximum operation frequencies. The first rows show the resources employed by each processing core and the ANN. The last row shows the total resources used by all FPGA-based processors for processing six signals at the same time in parallel. It can be deduced that the FPGA-based processor can be implemented easily in the selected FPGA and many other commercially available FPGA devices.

In Fig. 12, it can be seen the plots of mean, variance,

TABLE III  
CONFUSION MATRIX OF PQD CLASSIFICATION

PQD	C1	C2	C3	C4	C5	C6	C7	C8	C9	C10	C11
1	97	0	0	0	0	0	3	0	0	0	0
2	0	100	0	0	0	0	0	0	0	0	0
3	0	0	100	0	0	0	0	0	0	0	0
4	0	0	0	100	0	0	0	0	0	0	0
5	0	0	0	0	100	0	0	0	0	0	0
6	1	0	0	0	1	98	0	0	0	0	0
7	0	0	0	0	0	0	100	0	0	0	0
8	0	0	0	0	0	0	0	100	0	0	0
9	5	0	0	0	0	0	0	0	95	0	0
10	7	0	0	0	0	0	0	0	2	91	0
11	1	1	0	0	0	0	0	0	2	0	96

1: Pure signal. 2: Sag. 3: Swell. 4: Interruption. 5: Impulsive transient. 6: Oscillatory transient. 7: Voltage fluctuations. 8: Notching. 9: Harmonics. 10: Harmonics plus sag. 11: Harmonics plus swell.

skewness and kurtosis, for 60 minutes of the voltage signal of the first phase, and in Fig. 13 for 60 minutes of the current signal of the same phase. The plots of statistics of the voltage and the current signal statistics of the second phase are, respectively, in Fig. 14 and Fig. 15. Whereas the plots of statistics of the voltage and current signals of the third phase are in Fig. 16 and Fig. 17, respectively. In all figures, the blue

TABLE IV  
PQD HOS

PQD	Mean 1		Mean 2		Variance		Skewness		Kurtosis	
	$\mu$	$\sigma^2$	$\mu$	$\sigma^2$	$\mu$	$\sigma^2$	$\mu$	$\sigma^2$	$\mu$	$\sigma^2$
1	0.6468	0.0219	-0.6495	0.0248	0.5190	0.0349	-0.0018	0.0119	-1.4999	0.0001
2	0.3968	0.1792	-0.3502	0.1648	0.2006	0.1252	0.0450	0.1769	-1.4850	0.0373
3	0.8317	0.1712	-0.9033	0.1427	0.9519	0.2915	-0.0396	0.0932	-1.4958	0.0072
4	0.1992	0.2705	-0.0753	0.1554	0.0575	0.0815	0.1293	0.3400	-1.4316	0.0971
5	0.8475	0.2664	-0.2625	0.2605	0.5631	0.2639	0.0305	0.4393	-1.0175	0.4651
6	0.6311	0.0633	-0.6409	0.1354	0.7723	0.3049	-0.0653	0.6630	-0.2135	1.1323
7	0.6377	0.0161	-0.6346	0.0180	0.4997	0.0237	0.0025	0.0122	-1.4999	0.0011
8	0.6298	0.0044	-0.6270	0.0052	0.4939	0.0041	-0.0072	0.0084	-1.4900	0.0099
9	0.6874	0.0173	-0.6874	0.0173	0.5619	0.0253	0.0000	0.0000	-1.5682	0.1000
10	0.4572	0.2044	-0.3713	0.1811	0.2380	0.1467	0.0683	0.1842	-1.5457	0.1308
11	0.9081	0.1850	-0.9773	0.1626	1.0826	0.3476	-0.0292	0.0731	-1.5535	0.1053

1: Pure signal. 2: Sag. 3: Swell. 4: Interruption. 5: Impulsive transient. 6: Oscillatory transient. 7: Voltage fluctuations. 8: Notching. 9: Harmonics. 10: Harmonics plus sag. 11: Harmonics plus swell.

plots refer to the mean values of each specific statistic, and the red plots are the respective statistics, obtained by a sliding window over time.

In the case of the first phase, the statistics of the voltage

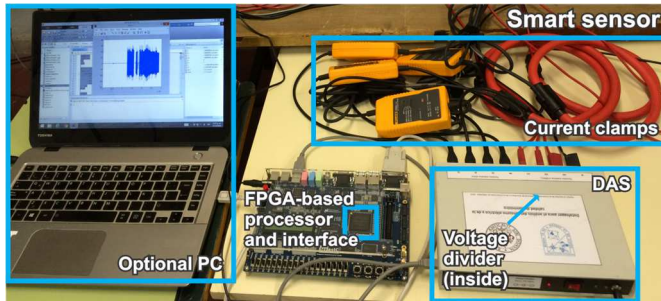


Fig. 11. Smart sensor in real operation.

TABLE V  
USAGE OF FPGA RESOURCES

Digital structure	Logic elements (%)	Registers (%)	Multiplier 9-bit (%)	Memory bits (%)	Max. Op. Freq.
Mean	249 (<1%)	131 (<1%)	2 (<1%)	0 (0%)	110 MHz
Variance	367 (<1%)	210 (<1%)	6 (1%)	0 (0%)	99.16 MHz
Skewness	2051 (2%)	1000 (1%)	35(7%)	73728 (2%)	58.75 MHz
Kurtosis	2162 (2%)	953 (1%)	40 (8%)	73728 (2%)	51 MHz
FFNN	2000 (2%)	580 (<1%)	4 (<1%)	153396 (4%)	61.75 MHz
<b>Total Processor</b>	<b>40974 (36%)</b>	<b>17244 (18%)</b>	<b>522 (98%)</b>	<b>1805112 (46%)</b>	<b>51 MHZ</b>

The percentages are rounded.

signal (Fig. 12) have mean values of -0.0011, 0.5000, -0.0002 and -1.4946, equal or very close to the expected values for sinusoidal signals at 0, 0.5, 0 and -1.5, respectively. The

standard deviation of each statistic plot is, respectively, 0.0004, 0.0052, 0.0009 and 0.0006. This situation, including that the resulting plots are relatively flat, indicates the absence of significant PQD. Only in the graph of the variance, a marked variation in its magnitude below and above the mean value is observed, which could indicate a sag and a swell, but this change is too small to be considered as a PQD. In the case of the current signal of the first phase (Fig. 13), the mean values of the statistics are 0.0002, 0.4994, 0.0400 and -0.8977, respectively, with standard deviations of 0.0007, 0.3466, 0.0560 and 0.3466, respectively. In the kurtosis plot, the peaks indicate the beginning or the end of a PQD. The magnitude changes in the variance indicate the presence of sags, swells or interruptions, while peaks indicate the presence of transients. Small and fast changes in the mean are due to harmonics, notching or voltage fluctuations. In the skewness, the magnitude changes and peaks indicate asymmetry in the signal waveform.

In the second phase, similar results to the first phase can be seen, especially for the voltage signal (Fig. 14), where there are no significant PQD. The statistics of the voltage signal of the second phase have mean values of 0.0011, 0.5000, -0.0002 and -1.4986, respectively, since the current signal of the same phase (Fig. 15) shows statistics with mean values of -0.0100, 0.4999, 0.0007 and -1.1771, respectively. In the case of the voltage signal, the statistics again have values very close to the expected values for a sinusoidal signal. This also applies to the current signal, except for the kurtosis. For the voltage signal, the standard deviation of each statistic plot is, respectively, 0.0004, 0.0054, 0.0009 and 0.0008, whereas for the current signals these are 0.0004, 0.0645, 0.0018 and 0.0362, respectively. It can be seen that although the mean values of the statistics of the current signal are close to the expected values, except for the kurtosis, the standard deviations are not very small, principally in the variance, indicating a high presence of peaks and changes in magnitude levels, indicating

the presence of PQD.

Again, the third phase results are similar to the results of the other phases. In the case of the voltage signal (Fig. 16), the mean values of the statistics are respectively, 0.0008, 0.5000, 0.0006 and -1.4947. The standard deviation of each statistic is respectively 0.0004, 0.0053, 0.0009 and 0.0006. The mean values of the statistics of the current signal are respectively

-0.0002, 0.5000, 0.0091 and -1.0722. It is clear that the mean value of the kurtosis is not the expected one for a sinusoidal signal. The standard deviation of each statistic is respectively 0.0004, 0.0381, 0.0022 and 0.0302. Again, the standard deviation of the variance is relatively big, because of the same reasons aforementioned.

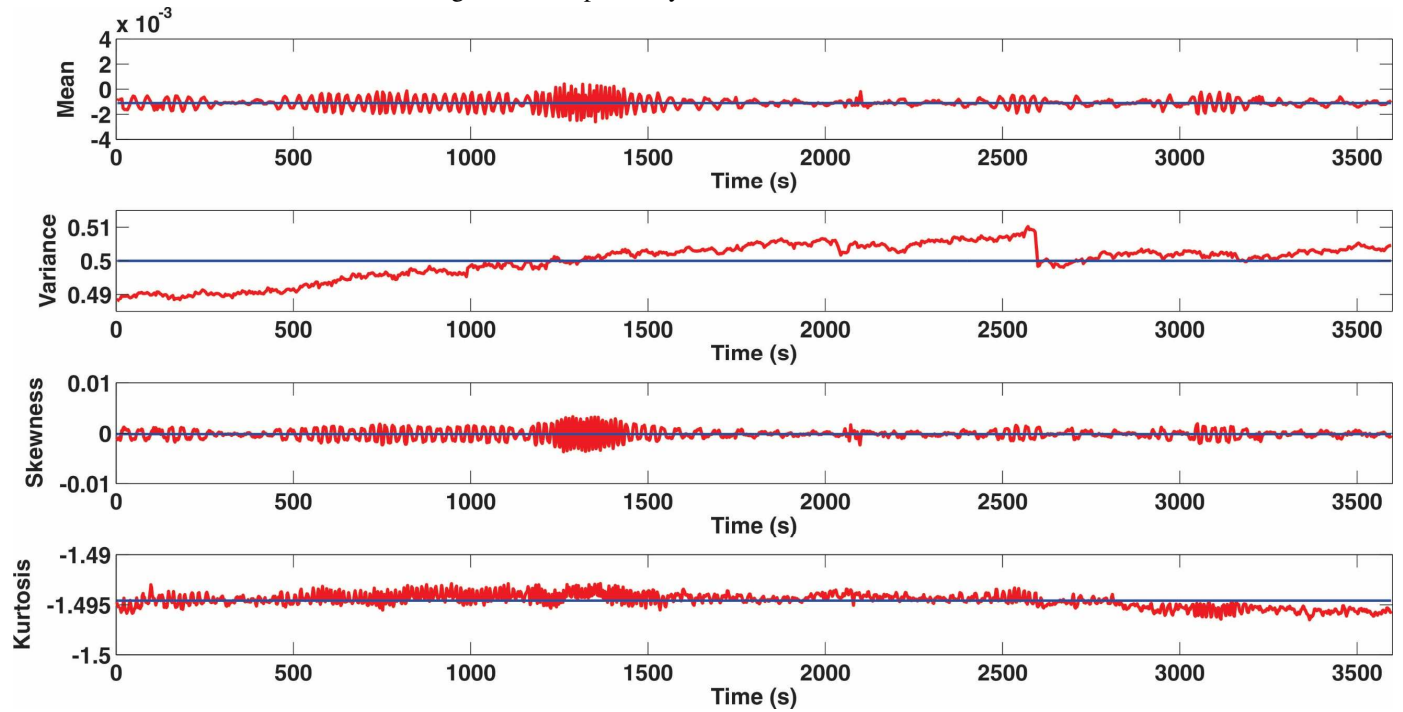


Fig. 12. Mean, variance, skewness and kurtosis of voltage signal of the first phase.

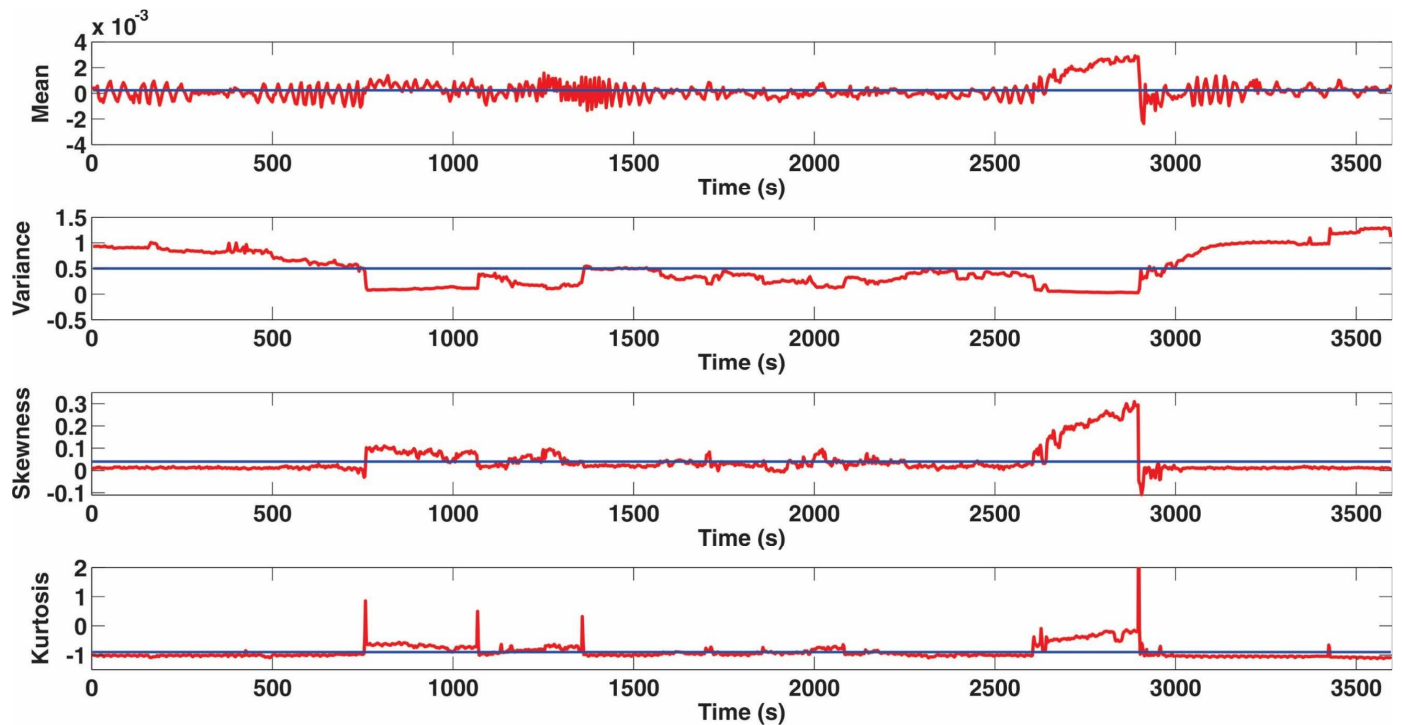


Fig. 13. Mean, variance, skewness and kurtosis of current signal of the first phase.

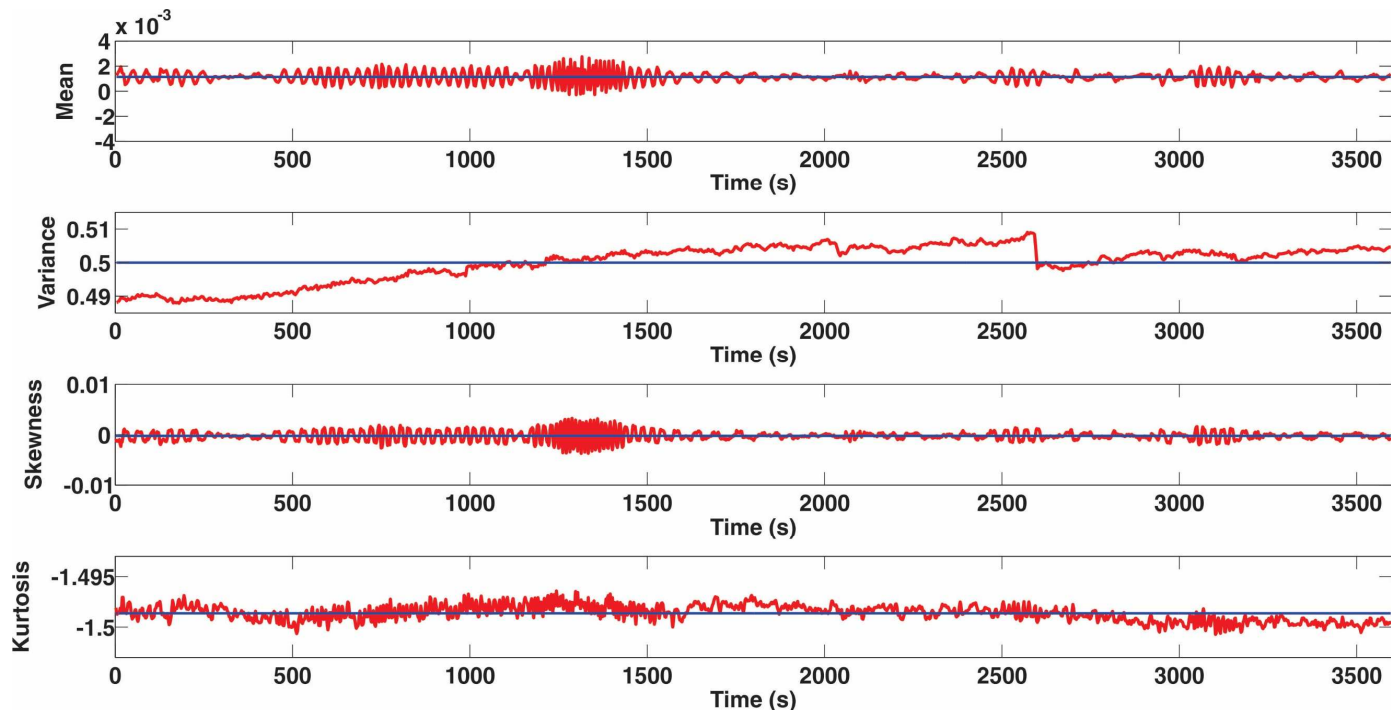


Fig. 14. Mean, variance, skewness and kurtosis of voltage signal of the second phase.

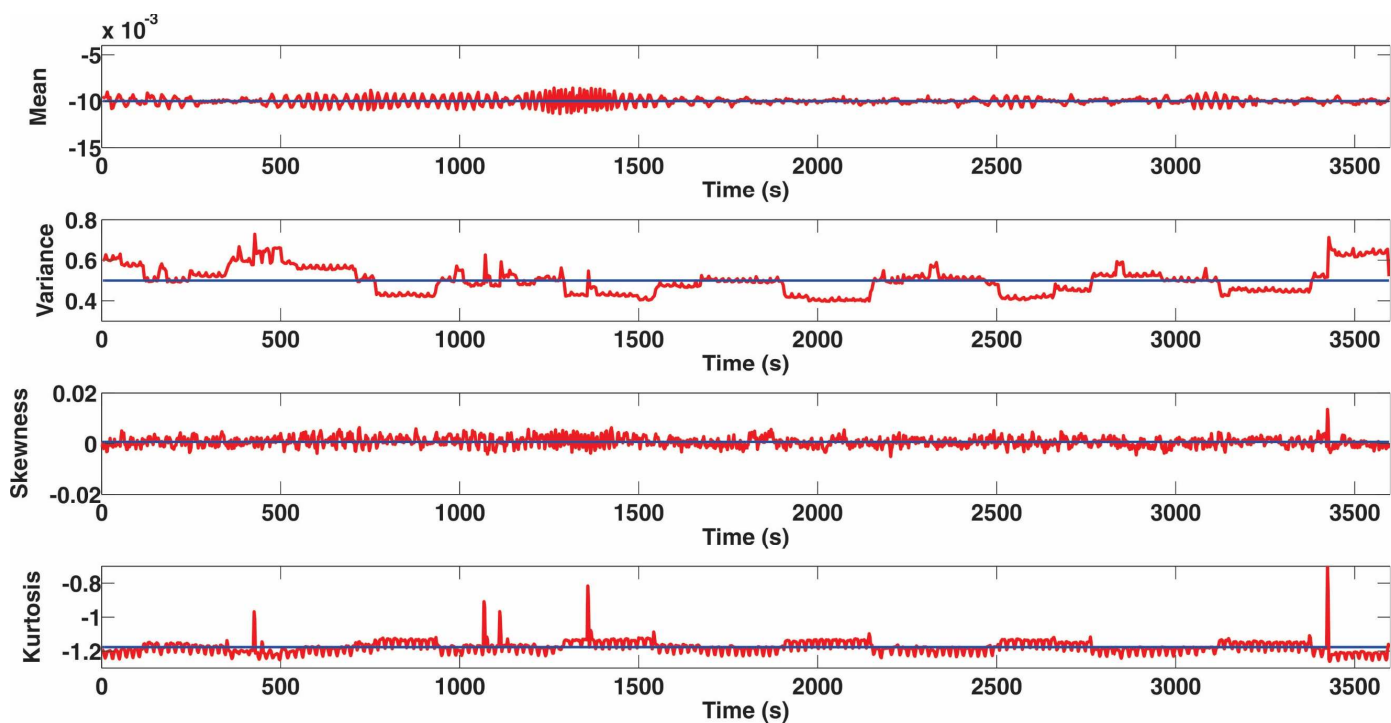


Fig. 15. Mean, variance, skewness and kurtosis of current signal of the second phase.

#### D. Analysis and discussion

From Table III, it can be seen that the majority of PQD are detected and classified correctly, with a total effectiveness of 97.9% in noiseless conditions. Sags, swells, interruptions, impulsive transients, notching and voltage fluctuations are the PQD best classified, all with an effectiveness of 100%. The worst results are obtained with pure signals and harmonics

conditions (harmonics, harmonics plus sag, and harmonics plus swell). In the case of the pure signals, those wrongly classified are sorted principally as voltage fluctuations, while the harmonics incorrectly classified are mainly sorted as pure signals. The decrease in the classification effectiveness of signals with harmonics is because the FFNN classifies the waveform and as it is well known that the different combinations of harmonics constitute different waveforms.

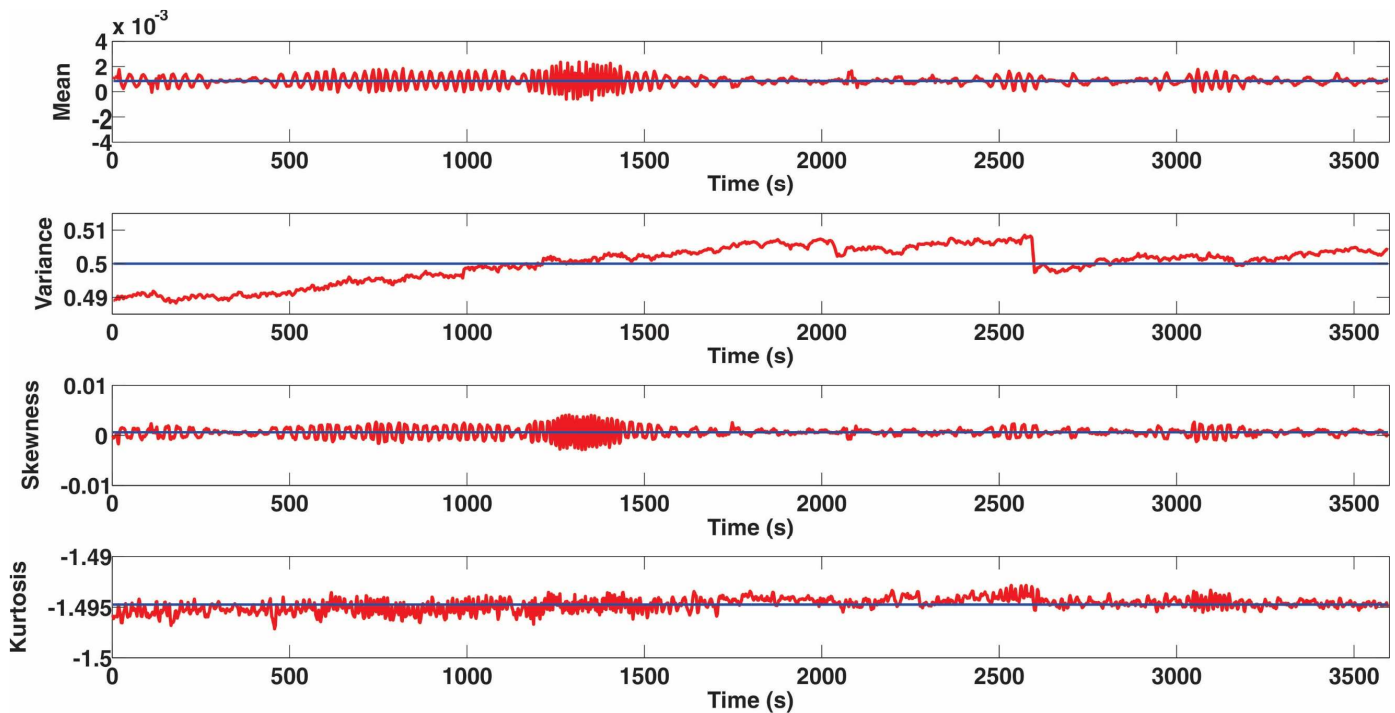


Fig. 16. Mean, variance, skewness and kurtosis of voltage signal of the third phase.

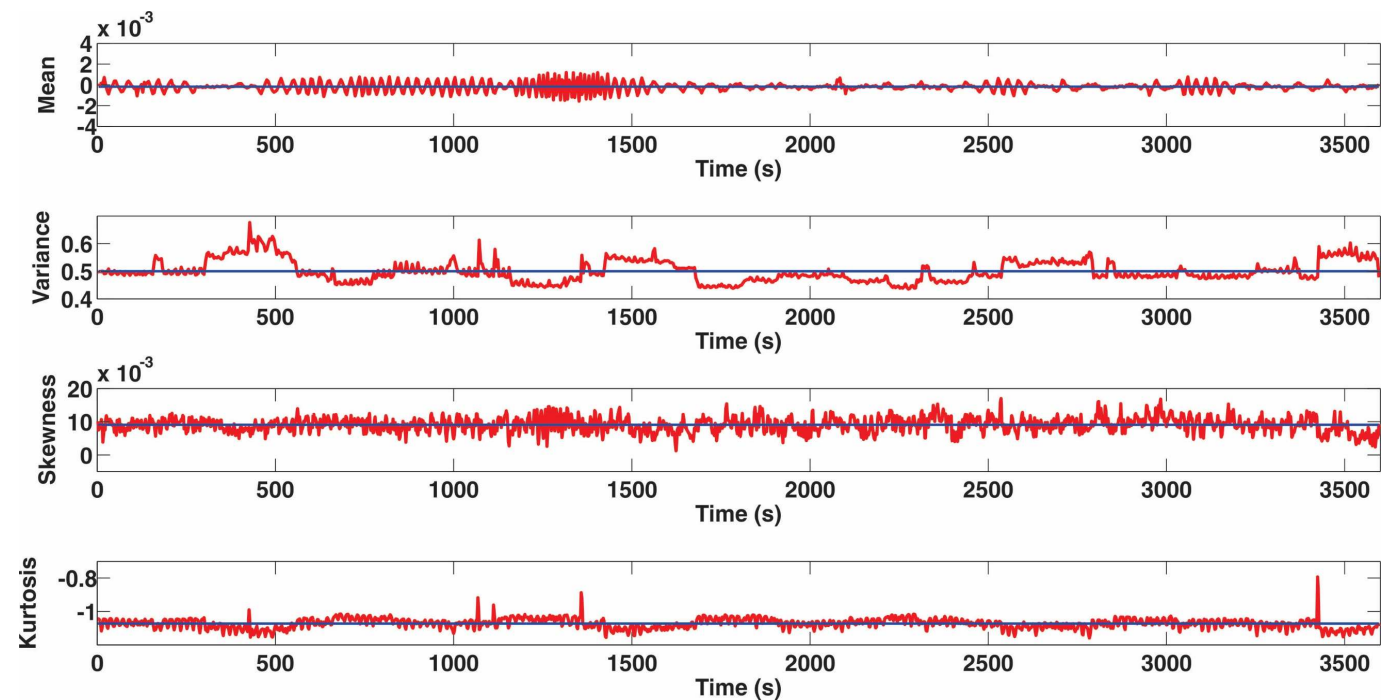


Fig. 17. Mean, variance, skewness and kurtosis of current signal of the third phase.

This also explains why the smart sensor does not work properly with noisy signals, including the fact that the chosen HOS features only help to describe the signal waveforms, not their spectral content.

Table IV shows the mean values and standard deviations of each HOS feature obtained from all synthetic PQD. A reference to the ideal values for a sinusoidal signal can be obtained from them, and how they vary according to each

PQD. In the case of the variance, it shows noticeable variations for the sags, swells, and interruptions, and to a lesser extent, but still clearly visible, for impulsive and oscillatory transients. The mean, computed for each half cycle, is also useful for the detection and quantification of the same PQD as the variance, except for the oscillatory transients. As previously stated, the skewness and the kurtosis can provide a measure of asymmetry. For this reason, these statistics are

useful for the detection and quantification of all PQD that distort the waveforms. As it can be observed in the HOS plots of the real signals, these two statistics indicate the presence of a transient, with one peak at the beginning of the transient and another at the end of the transient. During a transient like a sag, for example, the symmetry of the signal is lost in a fragment of the cycle. During the first transition, the negative semi-cycle presents a higher amplitude value than the positive semi-cycle; then, the skewness rapidly evolves towards negative values, showing a negative peak. At the end of the sag, it happens the other way around, so that the skewness turns positive, showing a positive peak. In the kurtosis, the two peaks are always positive. This is because, although the evolution of the amplitude values is different at the beginning and the end of the transient, the kurtosis identifies the deformation itself.

From the results obtained at the healthcare facilities, it is clear that the proposed smart sensor has been successfully tested in real conditions for PQ monitoring in a three-phase system. The voltage signals from the case study do not have a high presence of PQD. On the other hand, the current signals show more PQD content. The variance, skewness, and kurtosis are the statistics that give better information about the PQD presence and its PQ.

Finally, Table VI shows a comparison between the obtained classification results in this work and the reported results by other researchers. In noiseless conditions, this work shows better results than oldest works, and similar results compared to the latter works.

## V. CONCLUSIONS

This paper proposes a new smart sensor for online PQ monitoring and detection, and classification of PQD on electrical installations in a nonintrusive way, using only

voltage dividers and current clamps as primary sensors. It also shows the potential of an autonomous FPGA-based smart sensor and measurement system with the integrated capability of HOS processing. The system can be categorized as a high-performance waveform analyzer, a useful PQ monitoring system, and a precise PQD classifier, with the ability to classify eight different types of single PQD and two combinations of PQD. The HOS cores make use of very low FPGA resources, showing that this technology is well suited for the design and development of high-performance signal processing methods for smart sensors. This is one of the main advantages of this smart sensor, its great simplicity and low computational cost in comparison with other PQ monitoring systems and PQD classifiers. Another significant advantage of this smart sensor, compared to other smart sensors and reported methodologies, is that it can work online over three-phase power systems in parallel form with each phase at the same time.

The results show that the HOS and the traditional second order statistic (variance) are very useful for PQ monitoring and PQD detection. An ANN was used to achieve the PQD classification with a total effectiveness of 97.9%, but in future works, other options could be used with greater benefits, as SVM for example. The proposed methodology can be utilized for further research development in PQ monitoring by adding control tasks for each PQD. The experiment carried out under real operating conditions (in a healthcare facility) shows the validity and industrial applicability of the proposed smart sensor. Finally, this smart sensor could also be highly adaptable to other applications, like fault diagnosis in electrical machines, especially in induction motors, examining interactions between lines, and examining correlated events between monitoring points.

TABLE VI  
PERFORMANCE COMPARISON IN TERMS OF PERCENTAGE OF CORRECT CLASSIFICATION RESULTS

Year	2008		2009		2009		2011		2014		2014		2016		2017	
Reference	[39]		[40]		[41]		[36]		[42]		[43]		[44]		Proposed	
PQD	NL	N	NL	N	NL	N	NL	N	NL	N	NL	N	NL	N40	NL	N
Pure signal	100	-	-	-	96.15	98	-	-	-	-	-	-	-	-	97	-
Sag	98	-	-	-	100	100	98.46	-	100	-	-	-	-	92.75	100	-
Swell	92	-	100	-	100	100	100	-	98	-	-	-	-	96.45	100	-
Interruption	100	-	-	-	100	100	100	-	98	-	100	-	-	98.01	100	-
Impulsive transient	90	-	100	-	-	-	-	-	100	-	100	-	-	-	100	-
Oscillatory transient	100	-	97	-	97.94	92	100	-	96	-	100	-	-	94.36	98	-
Voltage fluctuations / Flicker	97	-	94	-	96.04	91	100	-	-	-	98	-	-	97.13	100	-
Notching	97	-	90	-	-	-	-	-	-	-	100	-	-	-	100	-
Harmonics	92	-	-	-	100	88	99.73	-	-	-	95.75	-	-	97.67	95	-
Harmonics plus sag	93	-	88	-	100	99	99.15	-	-	-	98	-	-	95.44	91	-
Harmonics plus swell	90	-	99	-	100	99	100	-	-	-	91.45	-	-	96.4	96	-

NL: noiseless signal. N: SNR of 20 dB, N40: SNR of 40 dB, -: not reported.

## ACKNOWLEDGMENT

The authors want to thank the administration board of Sanidad de Castilla y León (SACYL), Spain, for allowing the data acquisition from their healthcare facilities.

## REFERENCES

- [1] O.P. Mahela, A.G. Shaik, and N. Gupta, "A critical review of detection and classification of power quality events," *Renew. Sustainable Energy Rev.*, vol. 41, pp. 495–505, Jan. 2015.
- [2] IEEE Recommended Practice for Monitoring Electric Power Quality, IEEE Standard 1159, 2009.
- [3] Testing and measurement techniques power quality measurement methods, IEC 61000-4-30, 2003.
- [4] Voltage Characteristics of Electricity Supplied by Public Distribution Systems, Eur. Standard EN 50160, 1994.
- [5] D. Granados-Lieberman, R. J. Romero-Troncoso, R. A. Osornio-Rios, A. Garcia-Perez, and E. Cabal-Yepez, "Techniques and methodologies for power quality analysis and disturbances classification in power systems: a review," *IET Gener. Transm. Distrib.* vol. 5, no. 4, pp. 519-529, Apr. 2011.
- [6] A. Thapar, T. K. Saha, and Zhao Yang Dong, "Investigation of power quality categorisation and simulating its impact on sensitive electronic equipment," in *IEEE Power Engineering Society General Meeting 2004*, Denver, CO, USA, 2004, pp. 528-533.
- [7] C. Sankaran, *Power Quality*, CRC Press LLC, USA, 2002.
- [8] D. Granados-Lieberman, R.J. Romero-Troncoso, and R.A. Osornio-Rios, "Voltage drop repercussions in industrial processes due to the interaction of several machines in a manufacturing cell," *J. Sci. Ind. Res.*, vol. 72, pp. 746–753, Dec. 2013.
- [9] T. M. Galvão, F. N. Belchior, P. M. Silveira, and P. F. Ribeiro, "Comparative analysis of power quality instruments measuring voltage and power," in *2014 16th International Conference on Harmonics and Quality of Power (ICHQP)*, Bucharest, Romania, 2014, pp. 762-767.
- [10] B. A. Ahmad, H. H. ElSheikh, and A. Fadoun, "Review of power quality monitoring systems," in *2015 International Conference on Industrial Engineering and Operations Management (IEOM)*, Dubai, UAE, 2015, pp. 1-8.
- [11] S. Khokhar, A. A. B. Mohd Zin, A. S. B. Mokhtar, and M. Pesaran, "A comprehensive overview on signal processing and artificial intelligence techniques applications in classification of power quality disturbances," *Renew. Sustainable Energy Rev.*, vol. 51, pp. 1650-1663, Nov. 2015.
- [12] J. Rivera-Mejia, J. E. Villafuerte-Arroyo, J. Vega-Pineda, and R. Sandoval-Rodriguez, "Comparison of Compensation Algorithms for Smart Sensors With Approach to Real-Time or Dynamic Applications," *IEEE Sensors J.*, vol. 15, no. 12, pp. 7071–7080, Dec. 2015.
- [13] S. Mekid, "Further Structural Intelligence for Sensors Cluster Technology in Manufacturing," *Sensors*, vol. 6, no. 6, pp. 557–577, Jun. 2006.
- [14] K. Takahashi, and S Nozaki, "From intelligent sensors to fuzzy sensors," *Sens. Actuators A Phys.*, vol. 40, no. 2, pp.89-91, Feb. 1994.
- [15] J. Rivera, G. Herrera, M. Chacón, P. Acosta, and M. Carrillo, "Improved Progressive Polynomial Algorithm for Self-Adjustment and Optimal Response in Intelligent Sensors," *Sensors*, vol. 8, no. 11, pp. 7410–7427, Nov. 2008.
- [16] M. Chaudhari, and S. Dharavath, "Study of Smart Sensors and their Applications," *Int. J. Advanced Res. Computer Communication Engineering*, vol. 3, no. 1, pp. 5031–5034, Jan. 2014.
- [17] E. Monmasson, L. Idkhajine, M. N. Cirstea, I. Bahri, A. Tisan, and M. W. Naouar, "FPGAs in Industrial Control Applications," *IEEE Trans. Ind. Informat.*, vol. 7, no. 2, pp. 224-243, May 2011.
- [18] A. de la Piedra, A. Braeken, and A. Touhafi, "Sensor Systems Based on FPGAs and Their Applications: A Survey," *Sensors*, vol. 12, no. 12, pp. 12235–12264, Sept. 2012.
- [19] L. Ferrigno, C. Landi and M. Laracca, "FPGA-based Measurement Instrument for Power Quality Monitoring according to IEC Standards," in *2008 IEEE Instrumentation and Measurement Technology Conference*, Victoria, BC, Canada, 2008, pp. 906-911.
- [20] S. P. Valsan, and K. S. Swarup, "High-Speed Fault Classification in Power Lines: Theory and FPGA-Based Implementation," *IEEE Trans. Ind. Electron.*, vol. 56, no. 5, pp. 1793–1800, May. 2009.
- [21] D. Granados-Lieberman, M. Valtierra-Rodriguez, L. Morales-Hernandez, R. J. Romero-Troncoso, and R. A. Osornio-Rios, "A Hilbert Transform-Based Smart Sensor for Detection, Classification, and Quantification of Power Quality Disturbances," *Sensors*, vol. 13, no. 5, pp. 5507–5527, Apr. 2013.
- [22] N. K. Suryadevara, S. C. Mukhopadhyay, S. D. T. Kelly, and S.P.S. Gill, "WSN-Based Smart Sensors and

- Actuator for Power Management in Intelligent Buildings," *IEEE/ASME Trans. Mechatron.*, vol. 20, no. 2, pp. 564–571, Apr. 2015.
- [23] M. Valtierra-Rodriguez, R. A. Osornio-Rios, A. Garcia-Perez, and R. J. Romero-Troncoso, "FPGA-based neural network harmonic estimation for continuous monitoring of the power line in industrial applications," *Electr. Power Syst. Res.*, vol. 98, pp. 51–57, May 2013.
- [24] S. He, K. Li, and M. Zhang, "A Real-Time Power Quality Disturbances Classification Using Hybrid Method Based on S-Transform and Dynamics," *IEEE Trans. Instrum. Meas.*, vol. 62, no. 9, pp. 2465–2475, Sept. 2013.
- [25] J. M. Mendel, "Tutorial on higher-order statistics (spectra) in signal processing and system theory: theoretical results and some applications," *Proceedings of the IEEE*, vol. 79, no. 3, pp. 278–305, Mar. 1991.
- [26] J. J. González de la Rosa, J. M. Sierra-Fernández, A. Agüera-Pérez, J. C. Palomares-Salas, and A. Moreno-Muñoz, "An application of the spectral kurtosis to characterize power quality events," *Int. J. Electr. Power Energy Syst.*, vol. 49, pp. 386–398, Jul. 2013.
- [27] J. J. Gonzalez de la Rosa, A. Agüera-Pérez, J. C. Palomares-Salas, J.M. Sierra-Fernández, and A. Moreno-Muñoz, "A novel virtual instrument for power quality surveillance based in higher-order statistics and case-based reasoning," *Measurement*, vol. 45, no. 7, pp. 1824–1835, Aug. 2012.
- [28] V. Veena, and A. A. Kurian, "Classification of power quality disturbances using time/frequency domain features," in *2014 International Conference on Power Signals Control and Computations (EPSCICON)*, Thrissur, 2014, pp. 1-5.
- [29] Á. Quirós-Olozábal, J. J. González-de-la-Rosa, M. Á. Cifredo-Chacón, and J.M. Sierra-Fernández, "A novel FPGA-based system for real-time calculation of the Spectral Kurtosis: A prospective application to harmonic detection," *Measurement*, vol. 86, pp. 101–113, May 2016.
- [30] *American National Standard For Electric Power Systems and Equipment— Voltage Ratings (60 Hertz)*, ANSI C84.1, 2011.
- [31] S. Haykin, *Neural Networks and Learning Machines*, 3<sup>rd</sup> Edition, Pearson Prentice Hall, Ontario, Canada, 2008.
- [32] Y. Huang, "Advances in artificial neural networks – methodological development and application," *Algorithms*, vol. 2, no. 3, pp. 973–1007, Aug. 2012.
- [33] F. Chaibva, M. Burton and R.B. Walker, "Optimization of salbutamol sulfate dissolution from sustained release matrix formulations using artificial neural networks," *Pharmaceutics*, vol. 2, no. 2, pp. 182–198, Jun. 2010.
- [34] E. Cabal-Yepez, R. Saucedo-Gallaga, A. G. Garcia-Ramirez, A. A. Fernandez-Jaramillo, M. Pena-Anaya, and M. Valtierra-Rodriguez, "FPGA-Based Online Detection of Multiple-Combined Faults through Information Entropy and Neural Networks," in *2010 International Conference on Reconfigurable Computing and FPGAs*, Quintana Roo, Mexico, 2010, pp. 244–249.
- [35] *Fluke 434/435 Three Phase Power Quality Analyzer, User Manual*, Fluke, 2008.
- [36] J. G. M. S. Decanini, M. S. Tonelli-Neto, F. C. V. Malange, and C. R. Minussi, "Detection and classification of voltage disturbances using a Fuzzy-ARTMAP-wavelet network," *Electr. Power Syst. Res.*, vol 81, no. 12, pp. 2057–2065, Dec. 2011.
- [37] M. Uyar. S. Yildirim, and M. T. Gencoglu, "An expert system based on S-transform and neural network for automatic classification of power quality disturbances," *Expert Syst. Appl.*, vol. 36, no. 3, pp. 5962–5975, Apr. 2009.
- [38] *Cyclone IV Device Handbook*, Altera, 2016.
- [39] C. N. Bhende, S. Mishra, and B. K. Panigrahi, "Detection and classification of power quality disturbances using S-transform and modular neural network," *Electr. Power Syst. Res.*, vol. 78, no. 1, pp. 122–128, Jan. 2008.
- [40] B. Biswal, P. K. Dash, and B. K. Panigrahi, "Power Quality Disturbance Classification Using Fuzzy C-Means Algorithm and Adaptive Particle Swarm Optimization," *IEEE Trans. Ind. Electron.*, vol. 56, no. 1, pp. 212–220, Jan. 2009.
- [41] Z. Moravej, A. A. Abdoos, and M. Pazoki, "Detection and Classification of Power Quality Disturbance Using Wavelet Transform and Support Vector Machines," *Electr. Power Compon. Syst.*, vol. 38, no. 2, pp. 183–196, Dec. 2009.
- [42] Z. Liu, Q. Zhang, Z. Han, and G. Chen, "A new classification method for transient power quality combining spectral kurtosis with neural network," *Neurocomputing*, vol. 125, no. 11, pp. 95–101, Feb. 2014.
- [43] B. Biswal, M. Biswal, S. Mishra, and R. Jalaja, "Automatic Classification of Power Quality Events Using Balanced Neural Tree," *IEEE Trans. Ind. Electron.*, vol. 61, no. 1, pp. 521–530, Jan. 2014.

- [44] F. A. S. Borges, R. A. S. Fernandes, I. N. Silva, and C. B. S. Silva, "Feature Extraction and Power Quality Disturbances Classification Using Smart Meters Signals," *IEEE Trans. Ind. Informat.*, vol. 12, no. 2, pp. 824-833, Apr. 2016.



**Gerardo de J. Martinez-Figueroa** received the B.S. degree in communications and electronics engineering and the M.S. degree in electrical engineering from the University of Guanajuato, Salamanca, Mexico, in 2014 and 2017, respectively. He was an Intern with the University of Valladolid, Valladolid, Spain, in 2016. He is with the HSPdigital Research Group, Mexico. His research interests include hardware signal processing, digital systems and monitoring of power quality of electrical energy.



**D. Morinigo-Sotelo** (M'04) received the B.S. and Ph.D. degrees in electrical engineering from the University of Valladolid (UVA), Spain, in 1999 and 2006, respectively. He was a Research Collaborator on Electromagnetic Processing of Materials with the Light Alloys Division of CIDAUT Foundation since 2000 until 2015. He is currently with the Research Group in Predictive Maintenance and Testing of Electrical Machines, Department of Electrical Engineering, UVA and with the HSPdigital Research Group, México. His current search interests include condition monitoring of induction machines and power quality of electrical energy.



**Angel Luis Zorita Lamadrid** received the Ph.D. degree in Electrical Engineering from the University of Valladolid, Spain, in 2007, where he is a currently Full Professor at the School of Industrial Engineering and Director of the Electrical Engineering Department since 2012. He is a member of the research group ADIRE (analysis and diagnosis of facilities and electrical grids) in University of Valladolid, Spain, and his main research fields are power systems reliability, measurement and analysis of electric power quality, and electrical energy efficiency



**Luis Morales-Velazquez** (M'03) received the Ph.D. degree in mechatronics from the Autonomous University of Queretaro, Mexico, in 2010. He is a National Researcher level 1 with the Mexican Council of Science and

Technology, CONACYT. He is currently Professor with the Autonomous University of Queretaro, Mexico. He is author of more than 16 technical papers published in international journals and conferences. His fields of interest include hardware signal processing with FPGA and monitoring and diagnosis on dynamic systems.



**Rene de J. Romero-Troncoso** (M'07–SM'12) received the Ph.D. degree in mechatronics from the Autonomous University of Queretaro, Mexico, in 2004. He is a National Researcher level 3 with the Mexican Council of Science and Technology, CONACYT, and Fellow of the Mexican Academy of Engineering. He is currently a Head Professor with the University of Guanajuato and he has been an Invited Researcher with the Autonomous University of Queretaro, Mexico, and with the University of Valladolid, Spain. He is author of two books on digital systems (in Spanish), and a coauthor of more than 170 technical papers published in international journals and conferences. His fields of interest include hardware signal processing with FPGA and monitoring and diagnosis on dynamic systems. Dr. Romero–Troncoso was a recipient of the 2004 Asociación Mexicana de Directivos de la Investigación Aplicada y el Desarrollo Tecnológico Nacional Award on Innovation for his work in applied mechatronics, and the 2005 IEEE ReConFig Award for his work in digital systems. He is part of the editorial board of Hindawi's International Journal of Manufacturing Engineering.